

Verification of turbulent simulations using PoPe: quantifying model precision and numerical error with data mining of simulation output

Thomas Cartier-Michaud, Philippe Ghendrih, Guilhem Dif-Pradalier, Xavier Garbet, Virginie Grandgirard, Guillaume Latu, Yanick Sarazin, Frederic Schwander, Eric Serre

▶ **To cite this version:**

Thomas Cartier-Michaud, Philippe Ghendrih, Guilhem Dif-Pradalier, Xavier Garbet, Virginie Grandgirard, et al.. Verification of turbulent simulations using PoPe: quantifying model precision and numerical error with data mining of simulation output. Journal of Physics: Conference Series, 2018, 1125, pp.012005. 10.1088/1742-6596/1125/1/012005 . hal-02196674

HAL Id: hal-02196674
https://hal.science/hal-02196674

Submitted on 29 Jul 2019

HAL is a multi-disciplinary open access archive for the deposit and dissemination of scientific research documents, whether they are published or not. The documents may come from teaching and research institutions in France or abroad, or from public or private research centers.

L'archive ouverte pluridisciplinaire **HAL**, est destinée au dépôt et à la diffusion de documents scientifiques de niveau recherche, publiés ou non, émanant des établissements d'enseignement et de recherche français ou étrangers, des laboratoires publics ou privés.

Journal of Physics: Conference Series

PAPER • **OPEN ACCESS**

Verification of turbulent simulations using PoPe: quantifying model precision and numerical error with data mining of simulation output

To cite this article: Thomas Cartier-Michaud *et al* 2018 *J. Phys.: Conf. Ser.* **1125** 012005

View the article online for updates and enhancements.



IOP ebooks™

Bringing you innovative digital publishing with leading voices to create your essential collection of books in STEM research.

Start exploring the collection - download the first chapter of every title for free.

This content was downloaded from IP address 132.169.9.121 on 29/07/2019 at 10:19

IOP Conf. Series: Journal of Physics: Conf. Series **1125** (2018) 012005 doi:10.1088/1742-6596/1125/1/012005

Verification of turbulent simulations using PoPe: quantifying model precision and numerical error with data mining of simulation output

Thomas Cartier-Michaud[1], Philippe Ghendrih[2], Guilhem Dif-Pradalier[2], Xavier Garbet[2], Virginie Grandgirard[2], Guillaume Latu[2], Yanick Sarazin[2], Frederic Schwander[1], Eric Serre[1]

[1] M2P2, Aix-Marseille Universit, CNRS, F-13451 Marseille, France
[2] CEA, IRFM, F-13108 Saint-Paul-lez-Durance, France

E-mail: philippe.ghendrih@cea.fr

Abstract. Verification of a 1D-1V kinetic code with the PoPe method [1] is presented. Investigation of the impact of reducing the precision of the numerical scheme is analysed by following 3 indicators of the physics solved by the code, namely the plasma response to an external high frequency electric field wave. The response of the distribution function in the vicinity of the particle-wave resonance is found to be most sensitive to the resolution. Consistently, a rapid growth of the error indicator determined with PoPe is observed. However, no critical value of this indicator allowing us to retain the physics in a situation of degraded precision could be observed. The response of the amplitude of the electric potential fluctuations is characterised by a transient growth followed by a plateau. It is found that the loss of this plateau is governed by the resolution in v-space, but due to the generation of a symmetry in the problem rather than to errors in the numerical scheme. The analysis of the transient indicates that the growth rate of the amplitude of the electric potential is very robust down to very low resolution, step in velocity of 2 thermal velocities. However, a transition prior to this resolution, with step 0.5 thermal velocity, can be identified corresponding to a PoPe indicator of order zero, namely for errors of order 100 %.

1. Introduction

With the increasing computing capability, simulations are playing a growing role in research and innovation. Consequently, reliability of High Performance Computing must be addressed and quantifying each simulation quality becomes mandatory. Verification is usually performed on a small set of test cases, as in the Method of Manufactured Solution, which can depart from the conditions actually encountered in production runs. Projection on Proper elements, or PoPe [1], is a novel framework developed to quantify the simulation error, potentially for each production run. It requires typically 1% CPU overhead, some storage and post-processing, and is a powerful and versatile tool for verification: checking the implementation of models, determining the numerical convergence, and characterizing the residual error. The basic idea is to measure the departure from the expected bijection between the code data output and the set of equations that are considered to generate it.


Content from this work may be used under the terms of the Creative Commons Attribution 3.0 licence. Any further distribution of this work must maintain attribution to the author(s) and the title of the work, journal citation and DOI.
Published under licence by IOP Publishing Ltd

As an illustration PoPe is used to verify the 1D-1V VOICE code dedicated to investigating kinetic plasma physics [2]. In a standard fashion the VOICE code has been verified confronting the code output with analytical results on Landau damping, resonant interaction with an external electric field and collisional relaxation towards equilibrium temperature. Furthermore, each part of the code has been verified with the reference Method of Manufactured Solution. Kinetic problems have a unique feature insofar that they depend on a precise description of the phase space, including in particular the more challenging computation of the high velocity tail of the distribution function. However, standard quantities used for the physics, typically the electric field, are projections based on velocity integrals, and tend to smear out the high velocity contribution.

On more general grounds, one can use PoPe when investigating procedures to reduce the impact of the numerical errors, such as changing (i) the numerical method or its order, (ii) the mesh resolution or (iii) filtering the solution to only retain the contributions which are consistent with the precision of the numerical scheme. Cost and benefit of each improvement scheme can be analysed. Present development of PoPe in VOICE is focused on verification of the code on the fly, then providing a figure of merit of accuracy for each run of the code as a standard data output. This absolute criterion allows one to check that aspects (i) and (ii) are fulfilled.

The aim of this work is to address the situation where the PoPe figure of merit is degraded, hence suggesting significant numerical errors. Such a case is likely encountered when the required resolution exceeds the available computing capability. It is then important to determine a limit in the PoPe figure of merit beyond which some aspects of the simulation become questionable. In the case of an under-resolved simulation it is crucial to evaluate what part of the output can still be retained as significant for scientific purposes. Alternatively, one can address this problem as addressing a reduced model, the under-resolved simulation, to investigate the physics in the chosen conditions beyond the available computer resources. The question is then to evaluate how does this "numerically reduced" model do in matching the results of interest. A likely difficulty of working in such conditions is that the universality of the PoPe verification gives way to more open discussion on the code output where the criteria of interest play a major role. More detailed investigation of the code output is then required to assess the level of confidence for each particular observable.

In the present paper we consider the case of an electron population subject to an external electric field with given amplitude, frequency and wave vector in the frozen ions asymptotic limit. For weak amplitude of the electric field the resonant response of the electrons to the perturbation can be computed analytically, Section 2. We first show that this linear resonant response is recovered by the VOICE code while the version of the code used for the calculation is characterised by a PoPe indicator of zero, 100 % error, at high velocity, Section 3. With an improved version of the code, such that the numerical scheme does not produce such errors at large velocity, we then investigate the degradation of the numerical resolution when coarsening the mesh in velocity space, Section 4. Discussion and Conclusion close the paper, Section 5.

2. Electron response to an external high frequency electric field

In the simplest form, we thus address a 1D-1V kinetic model with the standard Vlasov-Poisson system. A Eulerian scheme, pseudo-spectral in both velocity and position directions, is used in the VOICE code for the work presented here and in Section 3. In Section 4, a finite difference scheme in the velocity direction is used instead of the pseudo-spectral one. With standard normalisation, plasma frequency for time, Debye length for length scales, reference density for the distribution function and thermal velocities for particle velocity, the set of equations for the

distribution function of the electrons $f_e(x, v, t)$ in the frozen ions asymptotic limit, is then:

$$\partial_t f_e + v\partial_x f_e + \partial_x\big(\phi + \phi_{ext}\big)\ \partial_v f_e = 0 \tag{1a}$$

$$\partial_x^2\phi(x,t) = \int dv f_e(x,v,t) - 1 \tag{1b}$$

Here $-\partial_x\phi_{ext}$ is the driving external electric field while ϕ the self-consistent electric potential induced in the plasma. In the literature, such externally driven Vlasov equation is also addressed as the KEEN wave [3, 4] (Kinetic Electron Electrostatic Nonlinear wave). However, the emphasis is then put on a second phase of self sustained self-organisation once the external drive is set back to zero.

The linear response, for small amplitude of ϕ_{ext}, has been analysed [5]. It is characterised by a resonant effect that can be seen in the amplitude of the electric potential generated by the plasma.

$$\widehat{\phi}(\omega,k) = -\frac{G_e(\omega/k, 0, f_{e,0})}{k^2 + G_e(\omega/k, 0, f_{e,0})}\ \widehat{\phi}_{ext}(\omega,k) \tag{2a}$$

This response is computed in Fourier space, $\widehat{\phi}(\omega,k)$ and $\widehat{\phi}_{ext}(\omega,k)$ being the Fourier transforms of the self-consistent and external electric potentials. The response function $G_a(\omega/k_a, \nu_a/k_a, f_a)$ for species a is defined by:

$$G_a(\omega/k_a, \nu/k_a, f_a) = \int dv\ \frac{1}{v - \omega/k_a - i\ \nu/k_a}\Big(-\partial_v f_a(v)\Big) \tag{2b}$$

where $k_a = k/\sqrt{m_a/m_e}$. For a Maxwellian distribution function, $f_a = f_M$ and dropping the subscript a, setting the restoring force at zero, $\nu = 0$, G is related to the plasma function $Z(z)$, $G(\sqrt{2}z, 0, f_M) = 1 + zZ(z)$. The time trace from the VOICE simulation is shown on Figure 1 for an amplitude of the drive of $|\widehat{\phi}_{ext}(\omega,k)| = 10^{-5}$. In the chosen case the linear analysis predicts an amplitude ratio, $A_G = |\widehat{\phi}(\omega,k)|/|\widehat{\phi}_{ext}(\omega,k)|$ of 8.4154, which appears to be in close agreement with that achieved in the VOICE simulation. Repeating such simulation at given k and varying ω allows one to determine the variation of A_G and compare it to the linear analysis, as shown on Figure 2.

One recovers expected features, at high frequency $\omega \gg 1$, the electron do not respond to the external field while in the adiabatic regime $\omega \ll 1$, there is an order 1 response. Near the plasma frequency one finds the resonant feature, with a Lorentzian-like shape. As expected for a Lorentzian, the resonance is also characterised by a change of phase by π between the low frequency regime, where the plasma electrons tend to screen the external electric potential, and the high frequency regime where the electric potential generated by the plasma tends to be in phase with the external drive.

The VOICE simulation data, black closed circles in Figure 2, is in very good agreement with the analytical formula. The numerical value of A_G is obtained by integrating the full non-linear Vlasov-Poisson system, Equation (1), with an external drive of amplitude $|\widehat{\phi}_{ext}(\omega,k)| = 10^{-5}$ at given wave vector k and case by case variation of the pulsation ω. After an initial transient, Figure 1, the amplification of the potential oscillations A_G is found to reach a steady state value. The latter is reported on Figure 2.

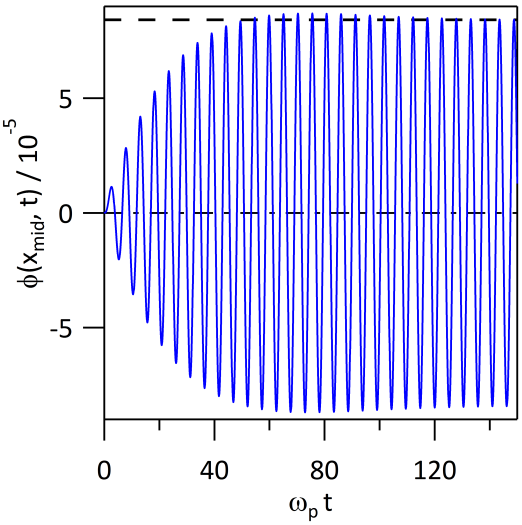


Figure 1. Time trace of the electric potential generated by the plasma, $\phi(x,t)$ normalised by the amplitude of the external drive, $|\widehat{\phi}_{ext}(\omega,k)| = 10^{-5}$, with $k = 1/2.8$, $\omega = 1.2$. The linear approximation yields the saturation level indicated by the thick dashed black line.

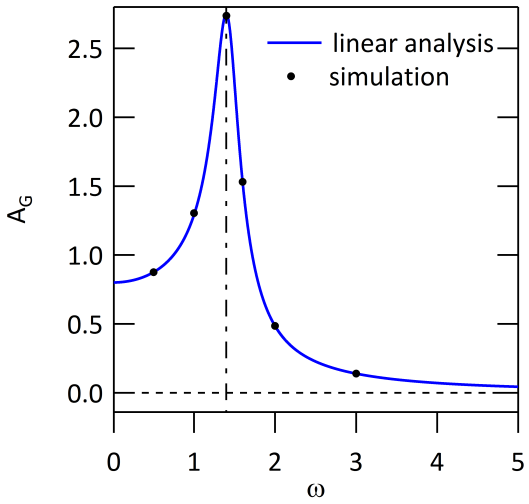


Figure 2. Amplitude ratio A_G between the potential generated by the plasma and that of the external drive for $k = 1/2$ as a function of ω. The linear approximation yields the blue curve, VOICE simulation are indicated by the closed black circles. The VOICE simulations are performed with $|\widehat{\phi}_{ext}(\omega,k)| = 10^{-5}$.

3. PoPe analysis of the numerical scheme

3.1. Short introduction to the PoPe verification method

For completeness we remind here the PoPe method for numerical scheme verification. On very general grounds numerical calculations solve equations of the form:

$$\mathcal{O}_c(X) = \sum_m a_m \mathcal{O}_m(X) \tag{3a}$$

where $\mathcal{O}_c$ is the computed operator depending on X and is equal to a linear combination of the generating operators $\mathcal{O}_m(X)$ with weight a_m. For simplification we shall consider here that all weights of the system are equal to 1, hence that actual numerical values of the control parameters are included in the definition of the operators $\mathcal{O}_m(X)$. In the case of Equation(1a), the space of calculation is 3D, $X = (x,v,t)$ and the right hand side operators are $\mathcal{O}_1(x,v,t) = -v\partial_x f_e(x,v,t)$ and $\mathcal{O}_2(x,v,t) = -\partial_x(\phi + \phi_{ext})\partial_v f_e(x,v,t)$. In-bedded in this definition of $\mathcal{O}_2(x,v,t)$ is the inversion of the Poisson equation (1b). The left hand side operator, the computed operator $\mathcal{O}_c$, is $\partial_t f_e(x,v,t)$. As apparent in the notation there is a lot in freedom in defining the operators. This property can be used at best for in-depth investigation of the numerical scheme. During the simulation run, the code output can be stored for a large number of points X. This data can then be used to reconstruct independently the set of operators $\mathcal{O}_m(X)$ as well as operator $\mathcal{O}_c(X)$. The PoPe overhead in computation is either the CPU time required for this recalculation on the fly, or storage capability for recalculation as post-processing.

As can be readily expected, a basic requirement of the operator recalculation is that this is performed at least with the same precision as done in the code for a given resolution in X. It

is important to stress that the decomposition in sub-operators can be carried to the point that each elementary operator can be verified independently.
Due to numerical approximations, the effective relation that is solved in the code is :

$$\mathcal{O}_c^{(s)}(X) = \sum_m a_m \mathcal{O}_m^{(s)}(X) \tag{3b}$$

$$\mathcal{O}_c^{(r)}(X) = \sum_m (a_m + \delta a_m)\mathcal{O}_m^{(r)}(X) + E(X) \tag{3c}$$

The equation solved numerically is (3b), the superscript (s) standing for simulation. The code output $\mathcal{O}_c^{(s)}(X)$ is compared to the reconstructed system, superscript (r). In equation (3c), the operators $\mathcal{O}_m^{(r)}(X)$ are the reconstructed operators and $E(X) = \mathcal{O}_c^{(r)}(X) - \mathcal{O}_c^{(s)}(X)$. Provided $\mathcal{O}_m^{(r)}$ are independently reconstructed and verified, one can consider them as a sufficient proxy for the actual operators $\mathcal{O}_m$ provided their numerical resolution is at least that implemented in the code. The numerical errors of the code can then be interpreted as errors of the projection of $\mathcal{O}_c(X)$ on the operators $\mathcal{O}_m$ leading to changes of the weights from a_m to $a_m + \delta a_m$ as well as the occurrence of a residual error $E(X)$, which by construction has zero projection on the generating operators $\mathcal{O}_m$. A least square method then allows one computing δa_m as well as statistics or dependences, for instance the evolution in time. The residual error can also be investigated. Making a projection of the latter on diffusion operators provides a means to actually check the often claimed but rarely quantified numerical diffusion. This has been done, indicating negligible diffusion in the numerical scheme of VOICE, but is not the scope of this paper.

3.2. PoPe verification of VOICE in v-Fourier space
Advancement in time in VOICE is performed with a fourth order Runge-Kutta scheme, hence a high order scheme with no specific conservation properties. Given periodic conditions in x, one readily considers Fourier modes in this direction as done for the linear analysis. The solution of the Poisson equation is then straightforward and corresponds exactly to that used in the linear analysis. The calculation of the non-linear term $\mathcal{O}_2(x, v, t) = -\partial_x(\phi + \phi_{ext})\partial_v f_e(x, v, t)$, if performed by inverse Fourier to real space, product in real space and back Fourier transform with standard pseudo-spectral code de-aliasing. It seemed appealing to perform also a Fourier transform in velocity space, hence implicitly "periodising" the distribution function in v using the same procedure to compute the two non-linear terms $\mathcal{O}_2(x, v, t)$ as well as $\mathcal{O}_1(x, v, t) = -\partial_x(v f_e)$. The rational for this choice of numerical scheme is that the filamentation governed by the convection part of the kinetic equation, $\partial_t f + v\partial_x f = 0$, for a mode k is position x leads to a phase $k\ x = k\ v\ t$, equivalently to a wave vector in velocity $K = k\ t$. A Fourier transform in velocity space seems therefore appropriate to follow the filamentation process exemplified by the relation $K = k\ t$.
It has been found that the error in the velocity direction of kinetic codes is rather specific [1]. The various errors determined by the PoPe projection are therefore analysed here retaining the velocity as a parameter, Figure 3.

Let us consider the advection operator $\mathcal{O}_1(x, v, t)$ and the error on its weight δa_1, which is also the relative error since $a_1 = 1$. The plot of δa_1 versus velocity, Figure 3, allows one identifying three regions. At small velocities the error is in the range or smaller than 10^{-6}, while at large velocities the error exceeds 1 for negative v and is of order 1 for positive v. In the intermediate range of values of v the error shoots up exponentially. One can remark also a loss of precision in the vicinity of $v = 0$ which can readily be understood since $\mathcal{O}_1(x, v = 0, t) = 0$. At the wave-particle resonance, where filamentation occurs, the scheme based on the Fourier transform in v-space is observed to be quite efficient, as illustrated by the dip in the error at $v/v_{the} = 3.6$

for the chosen parameters of this simulation.

Although the VOICE code seemed to be well verified by the linear calculation, as summarised in Figure 2, it thus appears that very significant errors exist in the high velocity regions. However, owing to the small weight of these regions in the moment of order zero used in the linear calculation, those errors have no visible impact in the verification against the linear analysis. A possible reason for the ill-behaviour of this numerical scheme could be some bump on tail instability. Indeed, in simulations, a noisy flat shoulder of the distribution function is observed to develop at largest velocity and gradually penetrates towards the low velocity. On finite times, this region thus extends, and can reach parts of the distribution of interest [5]. However, an issue solely governed by physics, would not be identified by PoPe as a numerical error. An alternative would be the accumulation of numerical errors on the large K modes (in v space). If these modes mostly shape the distribution in the vicinity of the vanishing derivative at maximum velocities, governed by the periodicity condition, then the error could lead to the phenomenology described above.
The code has been improved by switching to finite difference for the mesh in velocity with a fourth order scheme to compute the derivatives. The analysis with PoPe then indicates a significant improvement in accuracy, Figure 4. The high velocity regions now exhibit errors on the coefficient a_1 that are of the order of 10^{-4} while in the low velocity region the error if of order 10^{-7}, the dips being related to changes of sign of the δa_1. These features are readily observed at two different times $\omega_p t = 50$ and $\omega_p t = 100$. However, at the latter time, a change, and in particular an increase of the error, can be observed in the vicinity of the resonance, Figure 4. The finite difference scheme thus appears to be less efficient to handle the filamentation process at the wave-particle resonance. This effect is further discussed in Section 4. The increase of the error at high velocity can be observed to fit roughly a $|v|^4$ dependence, dashed black line

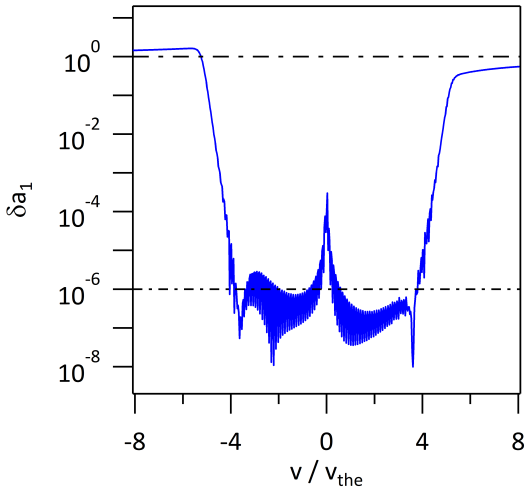


Figure 3. Velocity profile of the error on weight a_1, δa_1 for the version of VOICE with pseudo-spectral in v scheme. Simulation performed with $N_v = 2^9$ points in velocity space and $|\widehat{\phi}_{ext}(\omega, k)| = 10^{-5}$.

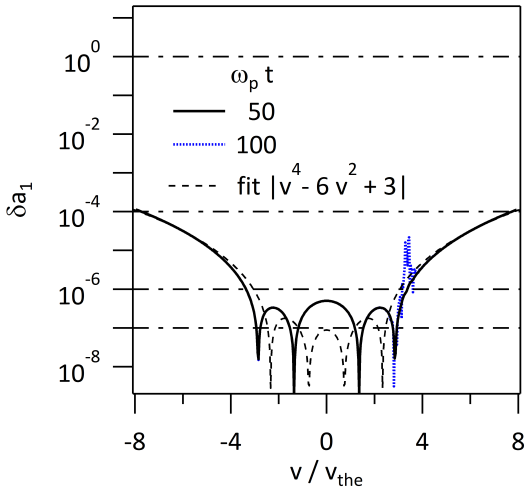


Figure 4. Velocity profile of δa_1 for the version of VOICE with finite difference scheme in v-space. Two times are presented, $\omega_p t = 50$ and $\omega_p t = 100$, plain black and dotted blue lines respectively, simulations with $N_v = 2^9$ points in velocity space and $|\widehat{\phi}_{ext}(\omega, k)| = 10^{-5}$.

on Figure 4, with additional effects governed by the changes of sign of the error δa_1 as well as an altogether different behaviour for the velocities of the bulk of the distribution function. The dependence in $|v|$ can be expected since both operators $\mathcal{O}_1(x,v,t) = -v\partial_x f_e(x,v,t)$ and $\mathcal{O}_2(x,v,t) = -\partial_x(\phi+\phi_{ext})\partial_v f_e(x,v,t) \approx \partial_x(\phi+\phi_{ext})v f_e(x,v,t)$ are typically proportional to v. The scaling with a power 4 is most likely governed by the order of the finite difference scheme used in velocity space, since for a Maxwellian $(\partial_v^4 f_e(x,v,t))/f_e(x,v,t) = v^4 - 6v^2 + 3$ for a Maxwellian. The fit plotted on Figure 4, $(v^4 - 6v^2 + 3)(\delta v)^4/(4!)/\sqrt{2}$, with $\delta v = 2v_{max}/N_v$, exhibits a qualitative agreement with the error on δa_1. The factor $1/\sqrt{2}$ has been introduced for a closer match. It is to be noted that the zeros are not located according to the approximation based on the fourth order derivative. However, the specific behaviour in the vicinity of the wave-particle resonance can distort the distribution function sufficiently to yield this difference. It seems therefore that the structure of the error δa_1, analysed here, can be driven by the fourth order scheme used for the derivatives by finite difference in the v-space. The difference between the implemented operator and the actual one would then simply be transferred into the variation of the weight δa, possibly with a splitting between the two errors δa_2 as well as δa_1.

4. Investigating the steps towards low resolution failure of VOICE simulations

4.1. Identifying key physics features

The dependence on mesh size is performed by changing $N_v = 2^N$. Let us consider as reference case the simulation with $N_v = 512$ (2^9, hence $N = 9$) points in velocity space, Figure 4. All simulations in the following are performed with a drive characterised by $k = 1/2.8$ and $\omega = 1.2$ and $|\widehat{\phi}_{ext}(\omega,k)| = 10^{-5}$. The phase velocity of the external wave is therefore $\omega/k = v_{res} = 3.36$. For $v_{max} = 8.09017$, the step in v is $\delta v \approx 0.03$, and the velocity point closest to the wave-particle resonance is at $v \approx 3.35$. Due to the wave feature of the drive and of the response, point in position space x behave identically with only a shift in time. Without loss of generality, one can then analyse all simulation output at a single location, we have chosen x_{mid} namely the

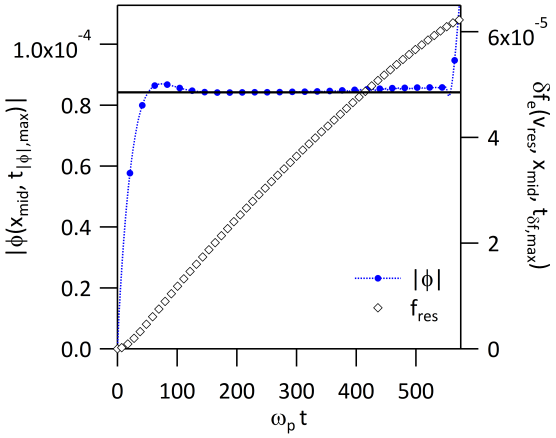


Figure 5. Quasi stroboscopic trace of the amplitude of the electric potential (Left Hand axis), blue dotted line with closed circle, symbol 1 point out of 8, and of the distribution function for $v - v_{res} < \delta v$ (Right Hand axis), open black square, symbol 1 point out of 2. The solid horizontal line corresponds to the analytical prediction.

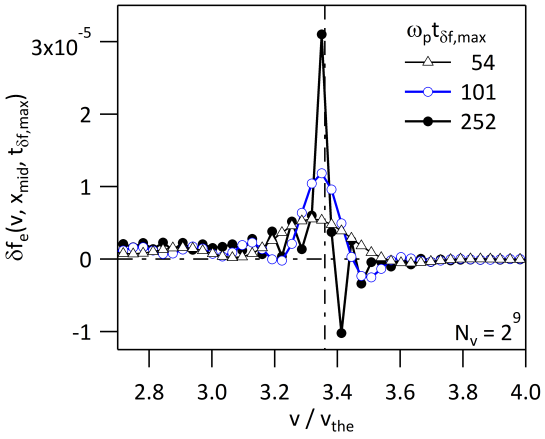


Figure 6. Velocity profile of $\delta f(x,v,t_{f,max}) = f(x,v,t_{f,max}) - f(x,v,0)$ in the vicinity of the wave particle resonance at three quasi-stroboscopic times defined according to the maximum of $\delta f(x_{mid},v,t)$ at $v = v_{res} - 0.01$, dashed-dot vertical line.

point in the middle of the x-domain. In such a case the transient regime to the quasi-steady state amplification of the electric potential is traced on Figure 1. The analysis of the plasma response is more conveniently analysed using the maxima of the amplitude of the oscillations of the signal of interest $f(x_{mid}, t_{g,max})$, where $t_{g,max}$ are the times where the field g goes through a local maximum governed by the oscillatory nature of the time dependence. The obtained data $|f(x_{mid}, t_{g,max})|$ is very close to a stroboscopic sampling at the period of the drive by the external electric field. However, the knowledge of $t_{g,max}$ allows one capturing the phase shift between the external drive and the field g as well as the small departure from the characteristic phase shift that appears to occur especially during the first oscillations. The result for the electric potential, $|\phi(x_{mid}, t_{|\phi|,max})|$, is plotted versus $t_{|\phi|,max}$, Figure 5, left hand axis with closed circles and dotted line. On this quasi-stroboscopic trace, one can observe the transient growth followed by a quasi-steady state flat-top and, towards the last points of the shown time window, a dip followed by a rapid growth. As will be discussed later, this change in behaviour is an artefact determined by the resolution in velocity space. Ignoring these features, one then observes a saturation of the growth of the amplitude of the plasma electric potential at a value comparable to that given by the analytical linear calculation. Conversely, the response of the perturbation of the distribution function $\delta f_e(x, v, t) = f_e(x, v, t) - f_e(x, v, t = 0)$ is found to be quite sensitive to the value of the velocity. Of particular interest is the behaviour in the neighbourhood of the resonant velocity v_{res}: $\delta f_e(v, x_{mid}, t_{\delta f,max})$ at velocity $v = 3.35 \approx v_{res}$. The response is close to a linear growth with no saturation, Figure 5, right hand axis, open black squares. For other velocities, in particular for the bulk of the distribution function, a behaviour comparable to that of the electric potential is observed. This is readily expected since the electric potential is the sum over all velocities of the distribution function, the most important terms in this sum must therefore exhibit the same behaviour as the electric potential. The response of the distribution function as well as the flattop of the electric potential amplitude or the transient are universal features of this model with a low amplitude drive. They appear to be well recovered in this

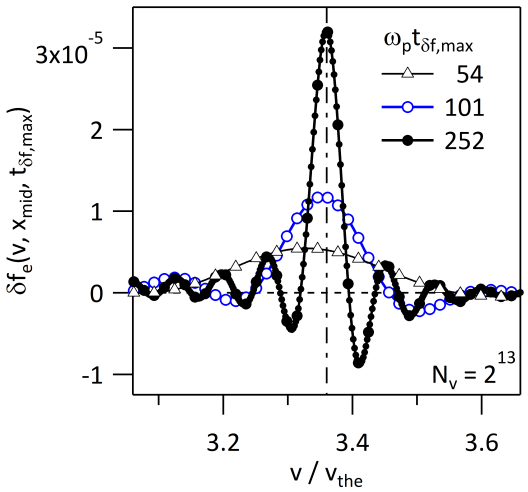


Figure 7. Velocity profile of $\delta f(x, v, t_{f,max}) = f(x, v, t_{f,max}) - f(x, v, 0)$ in the vicinity of the wave particle resonance at three quasi-stroboscopic times defined according to the maximum of $\delta f(x_{mid}, v, t)$ at $v = v_{res} - 2.9\ 10^{-4}$.

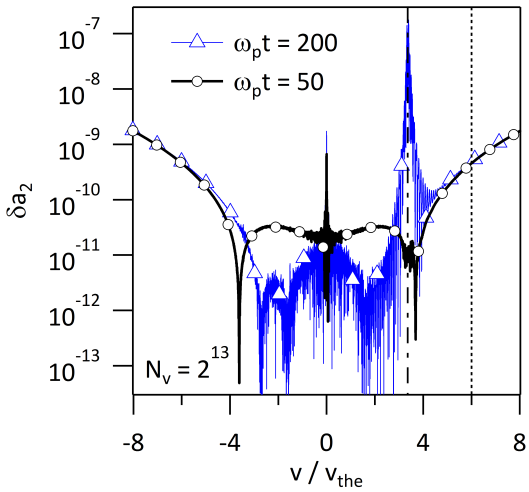


Figure 8. Velocity profile of δa_2. Two times are presented, $\omega_p t = 50$ and $\omega_p t = 200$, plain black line with open circles and plain blue line with open triangles respectively, simulations with 2^{13} points in velocity space.

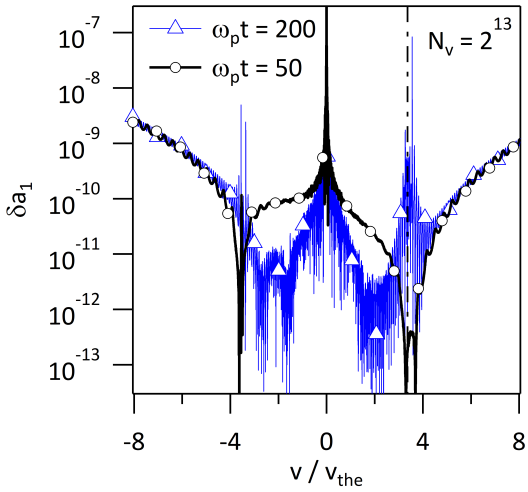


Figure 9. Velocity profile of the error on weight a_1, δa_1. Simulation performed with 8192 points in velocity space.

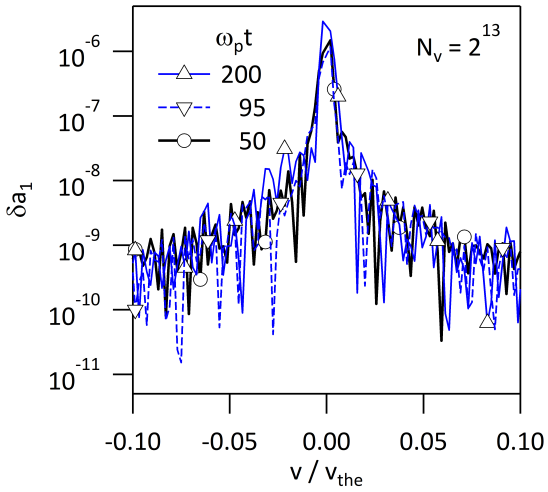


Figure 10. Profile of δa_1 in the vicinity of $v = 0$. Three times are presented, $\omega_p t = 50$, $\omega_p t = 95$, $\omega_p t = 200$, open circles, open down triangles and open up triangles respectively. Simulations with $N_v = 8192$ points.

reference case with resolution $N_v = 2^9$ points.

Let us now consider the evolution of the distribution function in the vicinity of the resonant velocity, Figure 6. The v-profile of $\delta f_e(x, v, t)$ is plotted at times when $\delta f_e(x_{mid}, v_{res}, t)$ is maximum, as in Figure 5. One can observe a smooth oscillation in v at time $t \approx 54$, curve with open triangle symbols on Figure 6. The amplitude and K_v wave vector of the oscillations are relatively small. The wave vector K_v is defined here such that $K_v \delta v = 2\pi$ where δv is the distance in velocity between two successive minima or maxima, typically a period. For this first case, one finds a period of 0.5 v_{the}, as observed on Figure 6, leading to $K_v \approx 12.6$. At a later stage, $t \approx 101$, the amplitude and K_v wave vector have grown. The amplitude has increased by a factor or order 2 and several periods in v are observed with $K_v \approx 42$. The structure in velocity appears to mostly develop towards the bulk velocities. Already at this stage, the maxima are rather triangular, hence with a single point describing the vicinity of the maximum. At still a later stage $t \approx 252$, the peak value at $v \approx v_{res}$ has further increased and K_v is typically $K_v \approx 100$. Regarding this result, the resolution limit suggested by this analysis seems to be reached for $\omega_p t \approx 100$. When considering the response of the distribution function in the vicinity of the resonant velocity, it thus appears that resolution issues can be observed well prior to the time when the amplitude of the electric potential departs from the predicted flattop, Figure 5.

When degrading or improving the resolution of the simulation with VOICE, we propose to confront the PoPe indicators with the three physical results discussed here, namely the flattop in the amplitude of electric potential fluctuations and its duration, the growth of this amplitude during the transient and finally the response of the distribution function in the vicinity of the resonance.

4.2. Impact of the resolution in velocity on the distribution function

We address here the evolution of the distribution function in the vicinity of the resonant velocity, $\omega/k = v_{res} = 3.36$ for the chosen case of the simulations, Figures 6 and 7. Reducing the step in v, by increasing the number of points at given minimum and maximum velocity yields, a clear improvement in the description of the distribution function in the vicinity of the resonance is observed for $N_v = 2^{13}$, Figure 7, compared to $N_v = 2^9$, Figure 6. For the times $\omega_p t = 54$, black curve closed triangles, and $\omega_p t = 101$, blue curve open circles, one finds several points per period, note that the symbols correspond to 1 point out of 8. Even at later time, $\omega_p t = 252$, black curve with closed circles, where the larger symbols correspond to one point out of 8 and the smaller closed circles to every point, the behaviour of the distribution function with these constraints is well resolved.

The profiles of the error δa_2 along v, at two different times and for $N_v = 2^{13}$, are plotted on Figure 8. The error profile is plotted for two times, an early time $\omega_p t = 50$, black curve open circles, and time $\omega_p t = 200$, blue curve open triangles. The vertical dash-dot line is localised at the resonance velocity and the dashed line at $v/v_{the} = 6$ a value used in the following. As for the error δa_1, Figure 4. One finds that the error is small, in the range of 10^{-11} for $|v|/v_{the} \leq 4$ corresponding to high accuracy, and increases with $|v|$ up to typically 10^{-9}. The overall dependence of the error is reminiscent of that on Figure 4, so that the same understanding holds. However, with time the error δa_2 increases by 4 order of magnitude in the vicinity of the resonant value $v_{res}/v_{th} = 3.36$, between $\omega_p t = 50$ and $\omega_p t = 200$. A similar analysis can be performed with the coefficient a_1 with a similar behaviour, Figure 9. For this coefficient the error in the vicinity of $v = 0$ is significant compared to other values of v. However, unlike the evolution of the error at v_{res}, the error in the vicinity of $v = 0$ does not vary significantly, as can be seen on Figure 10. This specific error for $v \approx 0$ can be understood since the associated operator $v\partial_x f$ vanishes for $v = 0$. This singularity tends to enhance the error on a_1. A similar trend occurs for a_2 since $\partial_v f$ also vanishes at $v = 0$ but is less pronounced.

The most striking aspect of analysis with PoPe is the evolution of δa_1 and δa_2 in the vicinity of the resonance. The traces of δa_1 and δa_2 are plotted on Figure 11 for $v \approx v_{res}$. Given the large variation of the error δa noticeable one Figures 8 and 9, the values plotted on Figure 11 and 12 are in fact the maximum of δa from $v_{res} - 3\delta v$ to $v_{res} + 3\delta v$, where δv is the step in v. These are labelled by $[\delta a]_{res}$. The dashed lines on Figure 11 are the values of δa at the resonance. The trends are similar for δa and $[\delta a]_{res}$. The error on a_1 is at least two order of magnitude smaller than that on a_2. The dips towards the small values corresponds to changes of sign. Comparing the traces for different values of N_v indicates that the latter behaviour depends on N_v. When analysing the error in terms of the resolution in v-space, the operator that depends on this mesh size is $\mathcal{O}_2 = -\partial_x(\phi + \phi_{ext})\partial_v f$. This operator being solved at order 4, the lowest order used in VOICE, one can expect the error δa_2 to be the largest. As can be seen on the profiles along v, Figure 8, rapid changes occur from one mesh point to the other. . For the two chosen values $N_v = 2^{11}$ and $N_v = 2^{13}$, the error exhibits a comparable behaviour, a nearly constant value, until a fast increase in time. In the latter regime, the growth of δa_2 scales typically like $t^{8.7}$. At lower precision, this exponent is found to be smaller, $t^{6.5}$ for $N_v = 2^9$. This still governs a very strong increase. The nearly constant error δa_2 in the early evolution times scales with N_v like N_v^{-4}, hence according to the order of the finite difference scheme, circle cross symbol $\oplus$ on Figure 12. The value reached by δa_2 at time $\omega_p t = 150$ is also found to scale like N_v^{-4}, symbols $\boxtimes$ on Figure 12. When considering the time needed to reach a critical value, $\delta a_2 = 10^{-5}$ in the chosen example, dash-dot line on figure 12, one finds that it scales roughly like $\sqrt{N_v}$. Consequently, for a prescribed value of the upper bound on the error δa_2, the duration of the simulated time with bounded error increases quite modestly with the number of points N_v along v.

In summary, the PoPe output in terms of the errors δa_1 and δa_2 indicates the build-up of an error at the resonance characterised by a rapid increase of the error for $\omega_p t \geq 70$. As such, it

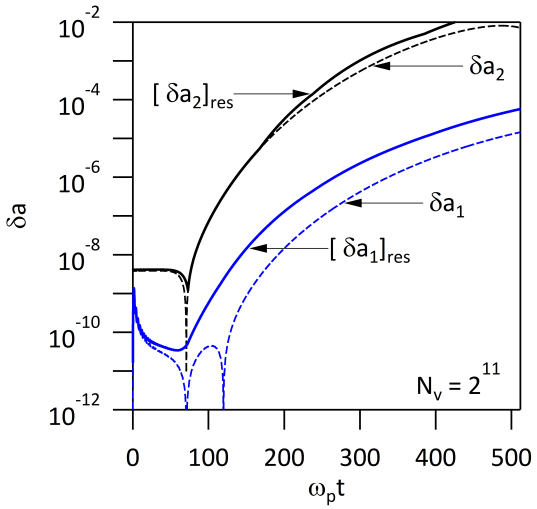


Figure 11. Traces of δa_1 and δa_2 for $N_v = 2^{11}$ mesh size in v-space, δa at the resonance, dashed lines, and $[\delta a]_{res}$ the maximum in its vicinity, plain line. The curve is not prolonged beyond $t = 512$, the error remaining large with no sign of saturation.

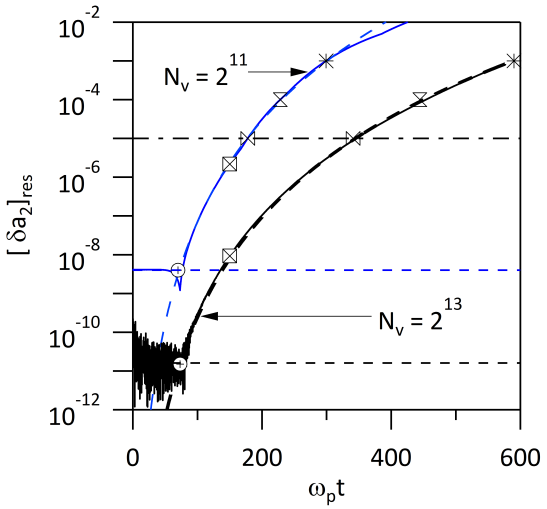


Figure 12. Comparing the error $[\delta a_2]_{res}$ (see text and Figure 11) for two different values of N_v. The symbols indicate the various characteristic values and times, the dashed horizontal line give the initial error level and the dashed curves of the fits with t^α, $\alpha \approx 8$.

is an indicator of an increase in numerical errors and consequently of a loss of accuracy in the description of the distribution function in the vicinity of the resonance. This is expected since the filamentation in v-space, namely the generation of small structure in v, is readily found to scale like $1/(kt)$ where k is the wave vector of the external electric field and t the evolution time. The limit of accuracy is therefore expected to be set by a relation of the form $\delta v\ k\ t \approx 1$, hence a limit in time of the form $t \leq 1/(k\ \delta_v)$. However, one cannot identify a change in the evolution of either δa_1 or δa_2 that would allow us setting an upper bound for the accuracy in the calculation. The only criterion of that form is obtained by defining *a priori* an upper bound on the error and determine the time required to reach this value. As discussed above this criterion indicates an increase of the simulation duration with the prescribed accuracy, but scaling as $\sqrt{N_v}$ and not N_v as suggested by the analysis of the filamentation process.

4.3. Impact of the resolution in velocity on the amplitude of the electric potential

A striking feature of the response to an external electric field in the linear regime is the plateau in of the electric potential generated by the plasma, Figure 1 and 5. One can then analyse the impact of the resolution in v-space on this plateau, Figure 13. One finds that the plateau in the amplitude of the fluctuations of the electric potential is lost earlier and earlier in time as the number of points in v is reduced. The loss is not observed for either $N_v = 2^{10}$ and $N_v = 2^{11}$, and it occurs at $\omega_p t \approx 600$ for $N_v = 2^9$, ≈ 300 for $N_v = 2^8$ and ≈ 150 for $N_v = 2^7$. For $N_v = 2^6$, the departure from the high precision curves occurs before the plateau is reached. It can then be argued that the physics at hand, the development of a plateau in the amplitude of the electric potential generated by the plasma, is only recovered when sufficient precision is v-space is achieved. The rough values given above suggest a scaling like N_v for the upper bound of validity in time. However it can be shown that this property is in fact akin to the bounce effect that is familiar in Landau damping. This effect occurs when $t\delta v = 2\pi$ hence when the initial phase in x is restored for all points of the mesh in v-space. This effect relies on

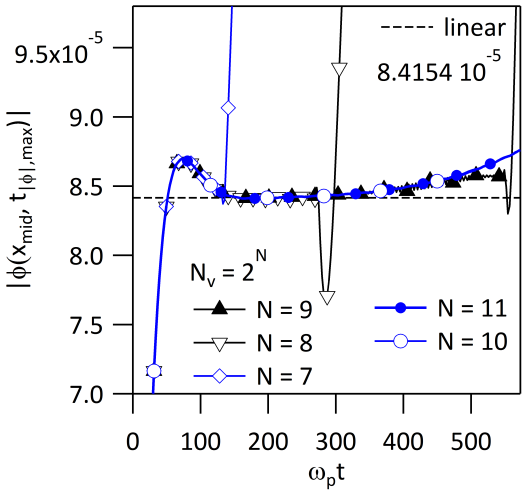


Figure 13. Trace of the amplitude of the oscillations of the electric potential zoomed on the value determined by the linear analysis, and for 5 different number of points in v-space, $N_v = 2^N$, $N \geq 7$.

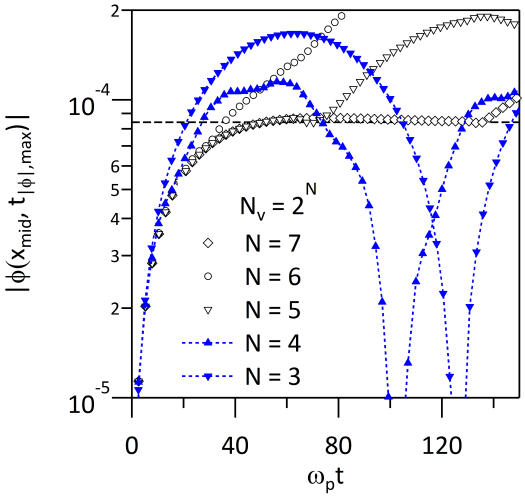


Figure 14. Trace of the amplitude of the oscillations of the electric potential in log scale for the low resolution cases, such that the linear saturation level is not recovered, for 5 different number of points in v-space, $N_v = 2^N$, $N \leq 7$.

the fact that a finite number of mesh points are used but more importantly that the scheme allows for such a periodicity. Remapping the points on different meshes in v in the course of the calculation would alleviate this issue. As a consequence, the loss of the plateau in the electric potential amplitude is driven by the use of a finite number of mesh points rather than by a loss of accuracy of the numerical scheme. Conversely, the fact that this bounce effect is observed indicates that he numerical scheme is accurate enough to recover the periodicity of the bounces in time as set by the relation $t\delta v = 2\ell\pi$, with $\ell \geq 1$. The identified issue in recovering the flat-top of the analytical calculation is not governed by numerical precision and is not therefore captured by the analysis with PoPe. When considering the results for the largest values of N_v on Figure 13, one can observe a gradual departure from the predicted saturation level. This effect is governed by particle trapping in the island formed in phase space in the vicinity of the resonance. This trapping time scales like $1/\sqrt{|\phi|}$, reducing the external drive thus allows one prolonging the plateau.

The other property of the evolution of the amplitude of the electric potential fluctuations is the growth regime from $t = 0$ to the flat-top that behave like $1 - \exp(-\gamma_L t)$ where $-\gamma_L$ is a Landau growth rate, Figure 14. In that plot one can readily observe the shortfall governed by the bounce effect, up to the stage where the bounce occurs during the transient growth. However, during the first times of the transient, the various traces appear to overlay even with the lowest resolution, $N_v = 2^3 = 8$, hence $\delta v = 2$ in units of thermal velocity since $v_{max} \approx 8$. To investigate this effect, we define $|\phi_{max}|(x_{mid}, t_j)$ which is the maximum amplitude of the j^{th} oscillation of $|\phi|$ at position x_{mid} which occurs at time t_j. The growth is then defined as $|\phi_{max}|(x_{mid}, t_j)/t_j$ since $\phi = 0$ at $t = 0$, Figures 1 and 14. Four curves display the results for the first, second, third and fourth consecutive maxima of $|\phi|$, Figure 15. One finds that the growth rate decreases slightly with step number, typically from 4.3 10^{-6} to 3.4 10^{-6}, a change of order 20 %. When varying N_v one finds that the growth rate is nearly constant down to $N_v = 32$, which onsets a change in behaviour with variations in the range of 5 % to 10 % of the

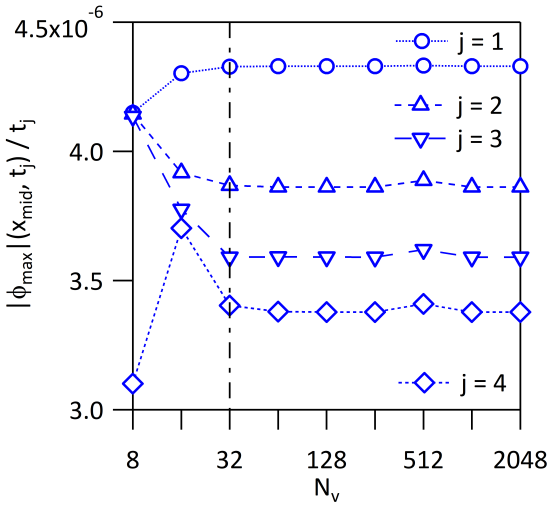


Figure 15. Variation of the growth rate of the amplitude of the electric potential during the transient sequence of the evolution with accuracy in v-space. The four first stroboscopic points are used. A change in behaviour is noticeable for $N_v \leq 32$ vertical dash-dot line.

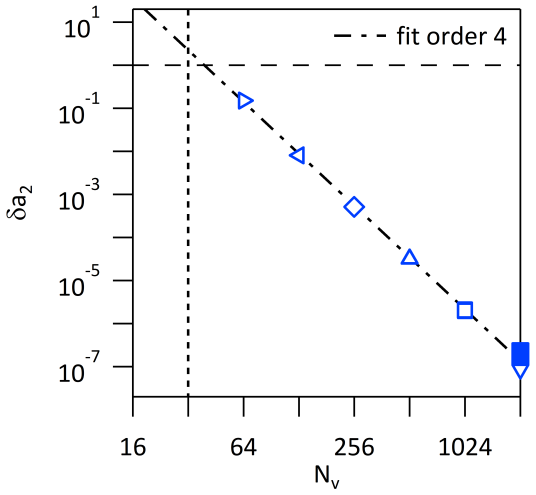


Figure 16. Dependence of δa_2 on the number of points in v-space, N_v, for $v/v_{the} = 6$. The data is fit by an order 4 variation. Note that all the points of the time trace are plotted, and observed to nearly superimpose, for each chosen value of N_v indicating quasi steady state behaviour.

growth rates. Although N_v can be seen as driving this rather clear change in behaviour, the effective changes in growth rate are rather small and hardly noticeable on Figure 14. It should also be underlined that, as the resolution is decreased, the distance of the nearest mesh point to the resonant velocity increases and the filamentation of the distribution function as depicted on Figures 6 and 7 is completely smeared out. Furthermore, the weight of the end points in v when computing the v-derivative increases quite significantly. Indeed, in the order 4 finite difference scheme the derivative computed at a given point depends on the two neighbouring points on both sides. Rather than reducing the order of the finite difference scheme or using non-centred difference schemes, we have set the v-derivative to zero for the two last points and at the two end points. The derivative is ill computed therefore on 4 points; for $N_v = 8$ this is half of the points, and the resonance then stands between the last point with properly computed derivative and the first point with imposed 0-derivative. One would therefore readily expect a strong departure with this resolution from higher resolution, while one observes in fact a clear difference but not a strong impact on the growth rate of the amplitude of the electric potential. Another consequence of this coding of the v-derivative is that the lower resolution, with $N = 2$ and therefore $N_v = 4$ does not model the Vlasov equation since the operator $\mathcal{O}_2(x, v, t) = -\partial_x(\phi + \phi_{ext})\partial_v f_e(x, v, t)$ is set at zero on all mesh points. The analysis of the data therefore appears to suggest a lower limit to N_v, $N_v > 32$ although the error on the growth rate remains small, indicating a very robust feature with little impact of the resolution in v.

In order to complete this analysis we investigate the error δa_2 in a region away from the resonance, here for $v/v_{th} = 6$, Figure 16. On this plot, all the data of the time trace of δa_2 is plotted for each value of the mesh resolution N_v. The vertical spread thus indicates the variation of δa_2 in time. In contrast to the vicinity of the resonance, one finds that the error is nearly constant. For each value of N_v one can therefore assign a time independent error. A forth order scaling of the error δa_2 at $v/v_{the} = 6$ with N_v is recovered, which is again consistent

with the fourth order scheme of the finite difference derivative. More interesting, in connection to the previous discussion, one finds $\delta a_2 \geq 1$ for $N_v \leq 32$, the error then exceeds 100 %.
Although the linear amplification regime of the external electric field appears to be very robust, and nearly independent of the mesh size in v, the analysis with PoPe suggests that an upper limit for the error δa corresponds to $\delta a \approx 1$, which occurs for $N_v < 32$, Figure 16. For $N_v = 64$, one finds an error given by PoPe in the range $\delta a \approx 0.1$. The growth rate of the potential is then quite comparable to values obtained with the highest resolution, Figure 15. This Vlasov-Poisson system in the linear regime thus appears to be very robust when reducing the precision along v. The only difficulty governed by such low resolution appears to be realignment of the initial perturbation on a time shorter than that required to reach the potential flat-top predicted by the linear analysis. This effect can certainly be alleviated by changing grid in v in order to remove the possible periodicity driving the bounce effect.

5. Discussion and Conclusion

The Pope framework is used for the verification on the fly of the code VOICE. We have shown that this method is precise and more complete than the rather standard verification based on the comparison with the linear analysis. For each simulation a figure of merit can be determined, namely the index I_{PoPe} computed as the minimum value of $-log_{10}(\delta a_j)$ considering all the operators labelled by j.
Compared to other methods used for verification, PoPe also provides a means to investigate precisely the numerical errors of the code. In particular it allows one to analyse the code precision for the physics that matter in the simulations. As shown in this paper, comparisons like matching the growth rates rely on integration on velocity space. Particular properties of wave-particle interaction can then exhibit large errors, not detected in the test on the growth rate if their weight in the integrals are too small. It is thus crucial to investigate the numerical errors in the production runs, in the regime of physics of interest. On the fly testing, as reported here for the VOICE code, are a step in that direction.
In the case of the kinetic code VOICE, one finds rather specific properties governed by the filamentation in velocity space, linear in time, so that the error increases with time. In order to identify changes in the PoPe criterion, that would be indicative of a loss of key physics, the accuracy in v-space is degraded from the reference cases with high precision. Three indicators of the physics are considered, the structure of the distribution function in the vicinity of the wave-particle resonance, the occurrence of saturation level of the amplitude of the electric potential oscillations, and the initial growth rate during the close to exponential transient prior to the saturation.
The Pope analysis for the Vlasov equation indicates that the profile in v of the error is comparable to the error term of the fourth order scheme that is implemented in VOICE to determine the derivative with respect to v of the distribution function. However, in the vicinity of the resonance the error is observed to exhibit a rapid increase with time, typically like t^8. As one would expect, the analysis with Pope thus indicates and demonstrates that resolution issues develop with the filamentation process.
When analysing the existence and duration of a saturation of the amplitude of the electric potential fluctuations, one finds that this feature is related to the number of points in v, but this effect is not governed by numerical errors. As for the known bounce effect in numerical solutions of Landau damping, the loss of the saturation of the amplitude of the electric potential is in fact induced by the restoration of the initial symmetry of the distribution function governed by the finite number of mesh points. Consequently the analysis with PoPe does not provide a particular signature for this effect. It is to be noted however that the loss of the plateau takes place when the error determined by PoPe at the wave-particle resonance has reached large values, typically $I_{PoPe} \leq 1$. Conversely, the analysis of the growth rate of the amplitude of the electric potential

does suggest that a lower bound must be considered for the number of points in v. It is also observed that this growth rate is robust down to very low resolution in v, step size δv equal to twice the thermal velocity. The critical value corresponds to the limit where errors of the order of 100 % are obtained, hence $I_{PoPe} = 0$. The safe side of this limit is characterised by errors of the order of 10 %. In terms of the index defined above $I_{PoPe} = 1$ is a lower limit beyond which even the very robust features of the physics deviate from their expected values.

Acknowledgements
This publication has been achieved with the support of the TOP project, which has received funding from Excellence Initiative of Aix-Marseille University- A*MIDEX, a French "Investissements d'Avenir" programme. This work has also been carried out within the framework of the EUROfusion Consortium and has received funding from the Euratom research and training programme 2014-2018 under grant agreement No 633053 for the project ESKAPE, WP17-ENR-CEA-01 as well as WP17-ENR-CEA-021 and WP17-ENR-CEA-03. The views and opinions expressed herein do not necessarily reflect those of the European Commission.

References

[1] Cartier-Michaud T, Ghendrih P, Sarazin Y, Abiteboul J, Bufferand H, Dif-Pradalier G, Garbet X, Grandgirard V, Latu G, Norscini C, Passeron C and Tamain P 2016 *Physics of Plasmas* **23** 020702 URL http://scitation.aip.org/content/aip/journal/pop/23/2/10.1063/1.4941974

[2] Valade L, Ekedahl A, Ghendrih P, Sarazin Y, Asahi Y, Bufferand H, Caschera E, Di Cintio P, Ciraolo G, Dif-Pradalier G, Donnel P, Garbet X, Giorgi P A, Grandgirard V, Latu G, Lepri S, Livi R, Nouri A and Serre E *Contributions to Plasma Physics* **58** 465–470 (*Preprint* https://onlinelibrary.wiley.com/doi/pdf/10.1002/ctpp.201700156) URL https://onlinelibrary.wiley.com/doi/abs/10.1002/ctpp.201700156

[3] Johnston W, Tyshetskiy Y, Ghizzo A and Bertrand P 2009 *Physics of Plasmas* **16** 042105

[4] Afeyan B, Casas F, Crouseilles N, Dodhy A, Faou E, Mehrenberger M and Sonnendrücker E 2014 *The European Physical Journal D* **68** 295

[5] Valade L, Caschera E, Ghendrih P, Sarazin Y and Ekedahl A 2016 *Journal of Physics: Conference Series* **775** 012015 URL http://stacks.iop.org/1742-6596/775/i=1/a=012015